Redox Biology 57 (2022) 102481

Contents lists available at ScienceDirect

Redox Biology

journal homepage: www.elsevier.com/locate/redox

Tauroursodeoxycholic acid functions as a critical effector mediating insulin sensitization of metformin in obese mice

Ya Zhang [a,b,1], Yang Cheng [a,1], Jian Liu [a,1], Jihui Zuo [a], Liping Yan [a], Ronald W. Thring [a], Xueqing Ba [c], Dake Qi [d], Mingjiang Wu [a], Yitian Gao [a,**], Haibin Tong [a,*]

[a] Zhejiang Provincial Key Laboratory for Water Environment and Marine Biological Resources Protection, College of Life and Environmental Science, Wenzhou University, Wenzhou, China
[b] Key Laboratory of Medical Genetics, School of Laboratory Medicine and Life Science, Wenzhou Medical University, Wenzhou, China
[c] Key Laboratory of Molecular Epigenetics of Ministry of Education, Northeast Normal University, Changchun, Jilin, China
[d] College of Pharmacy, University of Manitoba, Winnipeg, Canada

ARTICLE INFO

Keywords:
Metformin
Insulin resistance
Tauroursodeoxycholic acid
Nrf2
Bile salt hydrolase

ABSTRACT

Metformin is widely used to surmount insulin resistance (IR) and type 2 diabetes. Accumulating evidence suggests that metformin may improve IR through regulating gut microbiota and bile acids. However, the underlying mechanisms remain unclear. Our metabolomic analysis showed that metformin significantly increased the accumulation of tauroursodeoxycholic acid (TUDCA) in intestine and liver from high-fat diet (HFD)-induced IR mice. TUDCA also alleviated IR, and reduced oxidative stress and intestinal inflammation in *ob/ob* mice. TUDCA blocked KEAP1 to bind with Nrf2, resulting in Nrf2 translocation into nuclear and initiating the transcription of antioxidant genes, which eventually reduced intracellular ROS accumulation and improved insulin signaling. Analysis of gut microbiota further revealed that metformin reduced the relative abundance of *Bifidobacterium*, which produces bile salt hydrolase (BSH). The reduction in BSH was probably crucial for the accumulation of TUDCA. Metformin also increased the proportion of *Akkermanisia muciniphlia* in gut microbiota of *ob/ob* mice *via* TUDCA. These beneficial effects of metformin in remodeling gut microbiota, reducing oxidative stress and improving insulin sensitivity were partly due to the accumulation of TUDCA, suggesting that TUDCA may be a potential therapy for metabolic syndrome.

1. Introduction

Metformin is one of the major medications commonly used for the treatment of type 2 diabetes [1,2]. Metformin maintains glucose homeostasis through upregulating glucose uptake into peripheral tissues, such as the liver and skeletal muscle [3]. Molecular studies suggested that metformin activates AMP-activated protein kinase (AMPK) [4,5] which facilitates glucose uptake and glycolysis. However, oral administration of metformin leads to a higher concentration in the intestine compared to serum [6]. More interestingly, antibiotic treatments to diabetic mice significantly impair the pharmacological effects of metformin on reducing blood glucose levels [7]. These data together hint that the therapeutic efficacy of metformin on IR and T2DM might be impacted by intestinal metabolites and/or gut microbiota.

Indeed, gut microbiota and intestinal metabolites are highly correlated with the development of metabolic syndrome. Insulin sensitivity is promoted in patients with metabolic syndrome following transplantation of gut microbiota from lean healthy donors to obese subjects [8–10]. Bile acids are essential intestinal metabolites that not only promote the absorption of liposoluble nutrients but also regulate energy metabolism and homeostasis [11]. The alterations of bile acids are highly related to the metabolic phenotypes associated with IR in obese patients [12]. Certain types of bile acids suppress intestinal inflammatory responses and barrier dysfunction, and maintain intestinal homeostasis by modulating the gut microbiota [12–14]. These effects eventually improve metabolic syndrome but the molecular mechanisms are largely unknown.

Thus, in our present study, the next-generation sequencing and metabolomics technologies were applied to investigate the potential

* Corresponding author.
** Corresponding author.
E-mail addresses: gyt@wzu.edu.cn (Y. Gao), tonghaibin@gmail.com (H. Tong).
[1] These authors contributed equally to this study.

https://doi.org/10.1016/j.redox.2022.102481
Received 22 June 2022; Received in revised form 13 September 2022; Accepted 14 September 2022
Available online 15 September 2022

Abbreviations

T2DM	type 2 diabetes mellitus
AMPK	AMP-activated protein kinase
IR	insulin resistance
BA	bile acids
ER	endoplasmic reticulum
BSH	bile salt hydrolase
NASH	nonalcoholic steatohepatitis
ROS	reactive oxygen species
Nrf2	nuclear factor-erythroid-2-related factor 2
KEAP1	Kelch-like ECH-associated protein 1
TUDCA	tauroursodeoxycholic acid
IRS-1	insulin receptor substrate 1
Akt	protein kinase B
4-HNE	4-hydroxynonenal
IPGTT	intraperitoneal glucose tolerance test
IPITT	intraperitoneal insulin tolerance test
FFA	free fatty acids
FBG	fasting blood glucose
FINS	fasting serum insulin
HOMA-IR	homeostasis model assessment-estimated insulin resistance
2-NBDG	2-deoxy-2-[(7-nitro-2,1,3-benzoxadiazol-4-yl) amino]-D-glucose
NQO1	NAD(P)H:quinone oxidoreductase-1
HO-1	heme oxygenase 1
IL-1β	interleukin-1 β
Il-6	interleukin-6
OTU	operational taxonomic unit
TNF-α	tumor necrosis factor-α;
7α/β-HSDH	7α/β-hydroxysteroid dehydrogenase

mechanisms of metformin on modulating gut microbiota and metabolites in the intestine. Our findings will have important clinical implications for the development of novel pharmacological targets on the treatment of metabolic diseases.

2. Results

2.1. TUDCA is up-regulates in HFD-fed mice with intragastrical administration of metformin

The mice with HFD feeding for 20 weeks developed various metabolic dysfunctions including overweight, hyperglycemia, hyperlipidemia and glucose intolerance (Figs. S1A–K) which were reversed by metformin administration (Figs. S1A–K). The intestinal metabolites with or without metformin administration were measured by using lipid chromatography and mass spectrometry (LC-MS) (Fig. 1B). In the presence of metformin, 182 intestinal metabolites were upregulated while 118 metabolites were downregulated compared to the HFD group (Fig. 1C). Total 85 metabolites were significantly different between HFD and HFD + Met groups (Fig. 1D). Metformin significantly increased the intestinal content of taurine, choline and TUDCA (Fig. 1E). The level of TUDCA was also high in the serum and liver following metformin treatment (Fig. 1F). These data suggested that metformin upregulates conjugated bile acid TUDCA in HFD-fed mice.

2.2. TUDCA improves obesity and IR in *ob/ob* mice

To investigate the effects of TUDCA in alleviating IR and lipid accumulation *in vivo* (Fig. 2A), we treated *ob/ob* mice with TUDCA. TUDCA significantly alleviated the increase in body size and weight of the *ob/ob* mice (Fig. 2B and C), along with a correction in their total cholesterol (T-CHO), triacylglycerol (TG), and free fatty acids (FFA) in both liver and serum (Figs. S2A–C). Notably, TUDCA treatment tended to reverse the increase in FBS and FINS (Fig. 2D and E) as well as reduce HOMA-IR (Fig. 2F), an indicator for evaluating the level of IR. Further, TUDCA significantly improved glucose tolerance and IR in *ob/ob* mice, determined by IPGTT (Fig. 2G and H) and IPITT (Fig. 2I and J), respectively. The correction of insulin sensitivity is associated with the alteration of phosphorylation levels in Akt (Ser473) in the liver (Fig. 2K and L). Our results suggest that TUDCA resists the development of obesity and improves glucose homeostasis and insulin sensitivity.

2.3. TUDCA alleviates IR in palmitic acid (PA)-treated hepatocytes

Next, we investigated whether TUDCA could alleviate PA-induced IR in hepatocytes. In HepG2 cells, high PA (200 μM) decreased glucose uptake (Fig. 3A and B) and the phosphorylation of Akt at Ser473 and increased phosphorylation of IRS-1 at Ser307 (Fig. 3C–E). The impaired glucose uptake and insulin sensitivity caused by PA was significantly alleviated by TUDCA (Fig. 3F and G), but not choline and taurine (Figs. S3A–D) The same effects of TUDCA were also observed in primary mouse hepatocytes (Fig. 3H–J). These findings together suggested that TUDCA may resist high PA-induced insulin resistance in hepatocytes.

2.4. TUDCA alleviates IR by activating the Nrf2/ARE signaling pathway

Accumulating evidence suggests that oxidative stress is involved in the development of HFD-induced IR, in which metformin downregulates oxidative stress levels (Figs. S4A–G) in HFD-fed mice; thus TUDCA may play an important role in anti-oxidation. TUDCA intervention in *ob/ob* mice significantly increased hepatic and serum activity of CAT (Fig. 4A), as well as the ratio of GSH/GSSG in liver in *ob/ob* mice (Fig. 4B). The accumulation of lipid peroxide MDA was also significantly reduced by TUDCA intervention (Fig. 4C). Nuclear factor-erythroid-2-related factor 2 (Nrf2) is an important transcriptional factor in response to regulate the expression of phase II detoxifying and antioxidant enzymes. TUDCA significantly improved the translocation of Nrf2 into the nucleus (Fig. 4D) and subsequently up-regulated its downstream antioxidant genes, including *Nqo1, Ho-1* and *Gpx4* (Fig. 4E) in the liver from *ob/ob* mice. These data suggested that the Nrf2/ARE signaling pathway might be activated by TUDCA.

We further explore the efficacy and potential mechanisms of TUDCA in alleviating oxidative stress and IR in PA-treated hepatocytes. As shown in Fig. 5A and B, high PA-induced ROS generation in both primary mouse hepatocytes and HepG2 cells were attenuated by TUDCA, which was accompanied with an increased ratio of GSH/GSSG (Fig. 5C and D). Following high PA treatment, the suppression of the levels of Nrf2 expression and phosphorylation was reversed by TUDCA (Fig. 5E, Fig. S5). Accordingly, the expression of the antioxidant genes that are located at downstream of Nrf2/ARE signaling, *Ho-1*, *Nqo1*, and *Gpx4*, was also reversed (Fig. 5F). We found that in the absence of Nrf2 expression, TUDCA failed to alleviate PA-impaired glucose uptake in HepG2 cells (Fig. 5G and H, Fig. S6A) or primary cells isolated from $Nrf2^{-/-}$ mice (Fig. 5I and J, Fig. S6B). These data together suggested that TUDCA may enhance cellular antioxidant capacity and alleviate IR through activating the Nrf2/ARE signaling.

Kelch-like ECH-associated protein 1 (KEAP1) is a key protein that binds with Nrf2 resulting in the degradation of Nrf2. TUDCA attenuated the physical interaction of Nrf2 and KEAP1 and thus prevented Nrf2 from degradation (Fig. 5K). Molecular docking analysis was performed to explore the potential interaction between TUDCA and the Kelch domain of KEAP1. The theoretical three-dimensional binding mode of

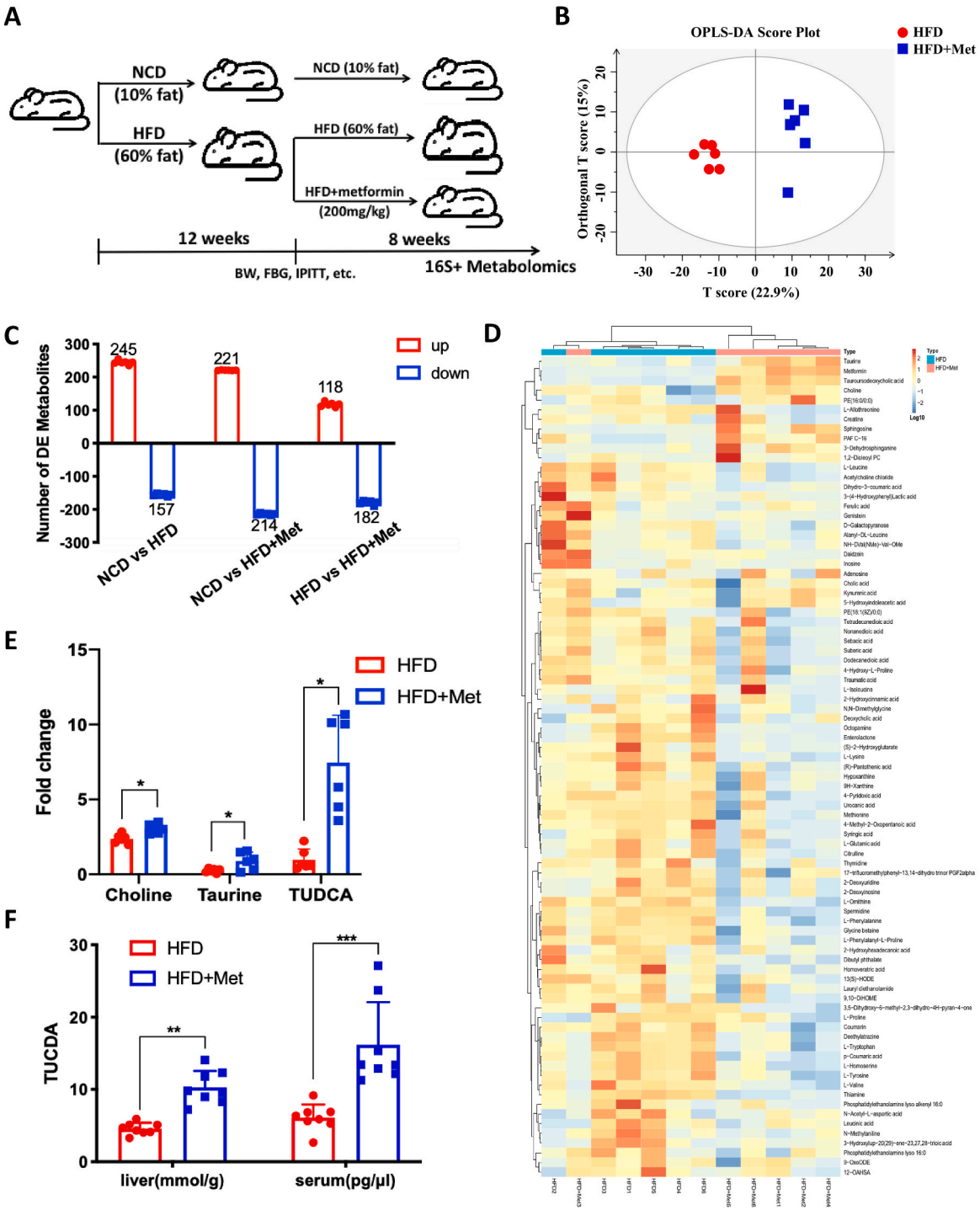

Fig. 1. TUDCA content was significantly increased by metformin in HFD-induced obese mice. (A) Schematic of animal experimental design. (B) OPLS-DA score plot of non-targeted metabolome. (C) Number of differential metabolites between each group. (D) Heatmap of 85 significantly differential metabolites. (E) The major upregulated differential metabolites in HFD + Met group. (F) The content of TUDCA in the liver/serum. Data are expressed as mean ± SD. $*P < 0.05$, $**P < 0.01$ and $***P < 0.001$ for HFD *vs* HFD + Met (n = 6). HFD, high fat diet; Met, metformin; OPLS-DA, orthogonal partial least-squared discriminant analysis; TUDCA, tauroursodeoxycholic acid.

the complex with the lowest docking energy is illustrated in Fig. 5L. The simulation results revealed that TUDCA was able to interact with the primary amino acid residues on the active site of KEAP1. TUDCA was positioned at the hydrophobic pocket, surrounded by the residues Val-418, Leu-557, Val-514, Val-561, and Thr-560, forming a stable hydrophobic binding. All those interactions helped TUDCA to anchor in the binding site of KEAP1, and the estimated binding energy of the KEAP1-TUDCA complex was found to be −10.21 kcal/mol. The docking simulation provided supportive evidence for TUDCA-induced Nrf2 activation and allowed us to predict the binding site in the Kelch domain. These results together indicated that TUDCA antagonizes the interaction between KEAP1 and Nrf2, leading to the prevention of Nrf2 from degradation and thereby its nuclear accumulation. As a result, the transcription of antioxidant enzymes that are of downstream of Nrf2 is upregulated, thus reducing oxidative stress and improving insulin signaling.

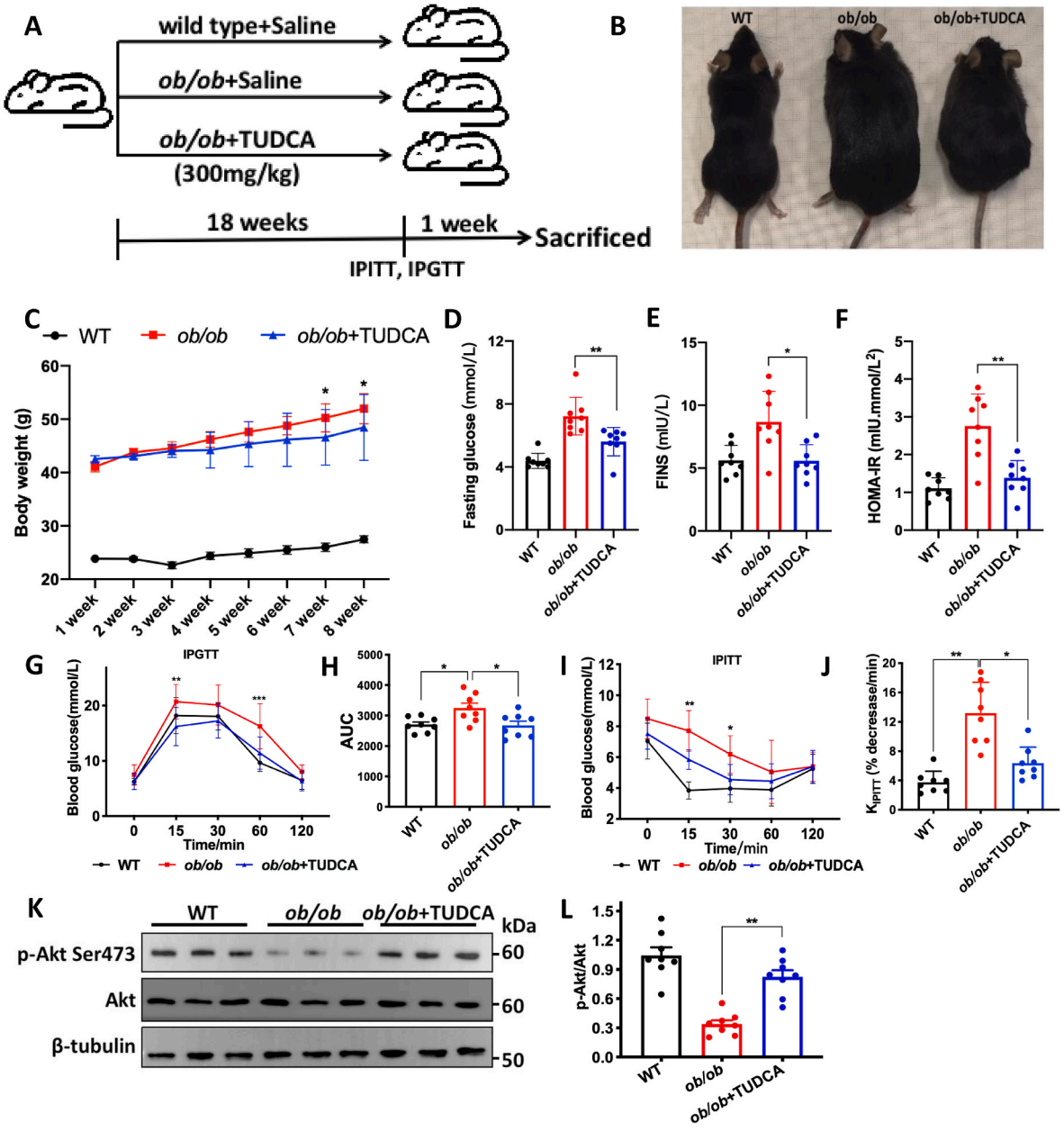

Fig. 2. TUDCA improves obesity and insulin resistance in *ob/ob* mice. (A) Schematic of animal experimental design. (B) Body size, (C) body weight, serum levels of (D) FBG and (E) FINS, (F) HOMA-IR. Mice, fasted overnight and fasted for 6 h, were injected with glucose (2 g/kg in saline) or insulin (0.75 IU/kg in saline) for IPGTT or IPITT, respectively. (G) IPGTT and (H) AUC of IPGTT, (I) IPITT and (J) the slope of IPITT are shown. (K) Protein expression of p-Akt and Akt in liver and (L) the quantitative analysis for the densitometry. Data are expressed as mean ± SD. $^{*}P < 0.05$, $^{**}P < 0.01$ and $^{***}P < 0.001$ for *ob/ob* vs *ob/ob* + TUDCA (n = 8). AUC, area under the curve; FBG, fasting blood glucose; FINS, fasting serum insulin; HOMA-IR, homeostatic model assessment for insulin resistance; IPGTT, intraperitoneal glucose tolerance test; IPITT, intraperitoneal insulin tolerance test; TUDCA, tauroursodeoxycholic acid.

2.5. Metformin increases the accumulation of TUDCA through remodeling gut microbiota

To further examine the potential mechanisms by which metformin regulates TUDCA levels in HFD-fed mice, fecal samples were collected for gut microbiota analysis through 16S rRNA amplicon sequencing. Metformin significantly increased the Ace and Chao1 indices in the HFD group (Table 1), but clustered partially apart from HFD-fed mice samples (Fig. 6A, Fig. S7A), suggesting an important change in gut microbial profile. The reduction in Bacteroidetes (Fig. S7B) and the increase in the Firmicutes/Bacteroidetes ratio induced by HFD, which are two hallmarks of obesity-driven dysbiosis, were also prevented by metformin administration (Fig. S7C). Based on FunGuild and FAPROTAX analysis of microbiota function, the HFD group had a reduced proportion of the chemoheterotrophy and the fermentation bacteria compared with the normal chow (NCD) group (Fig. S7D). However, metformin reshaped the structure of gut microbiota, upregulated the proportion of chemosynthetic and fermentative bacteria.

Heatmap presented the clustering of bacterial communities with their relative abundances at the genus level (Fig. 6B). We found that compared with the NCD group, unique high-abundance bacteria in the HFD group were mainly concentrated in *Bifidobacterium, Roseburia, Lachnoclostridum, Alloprevotella* and *Mucispirilum*. However, metformin decreased the abundance of these bacteria. Metformin also specifically increased the abundance of *Butyricimonas, Parasulterella, Parabacteroides* and *Akkermansia*. Consistent with the reduce in Firmicutes/

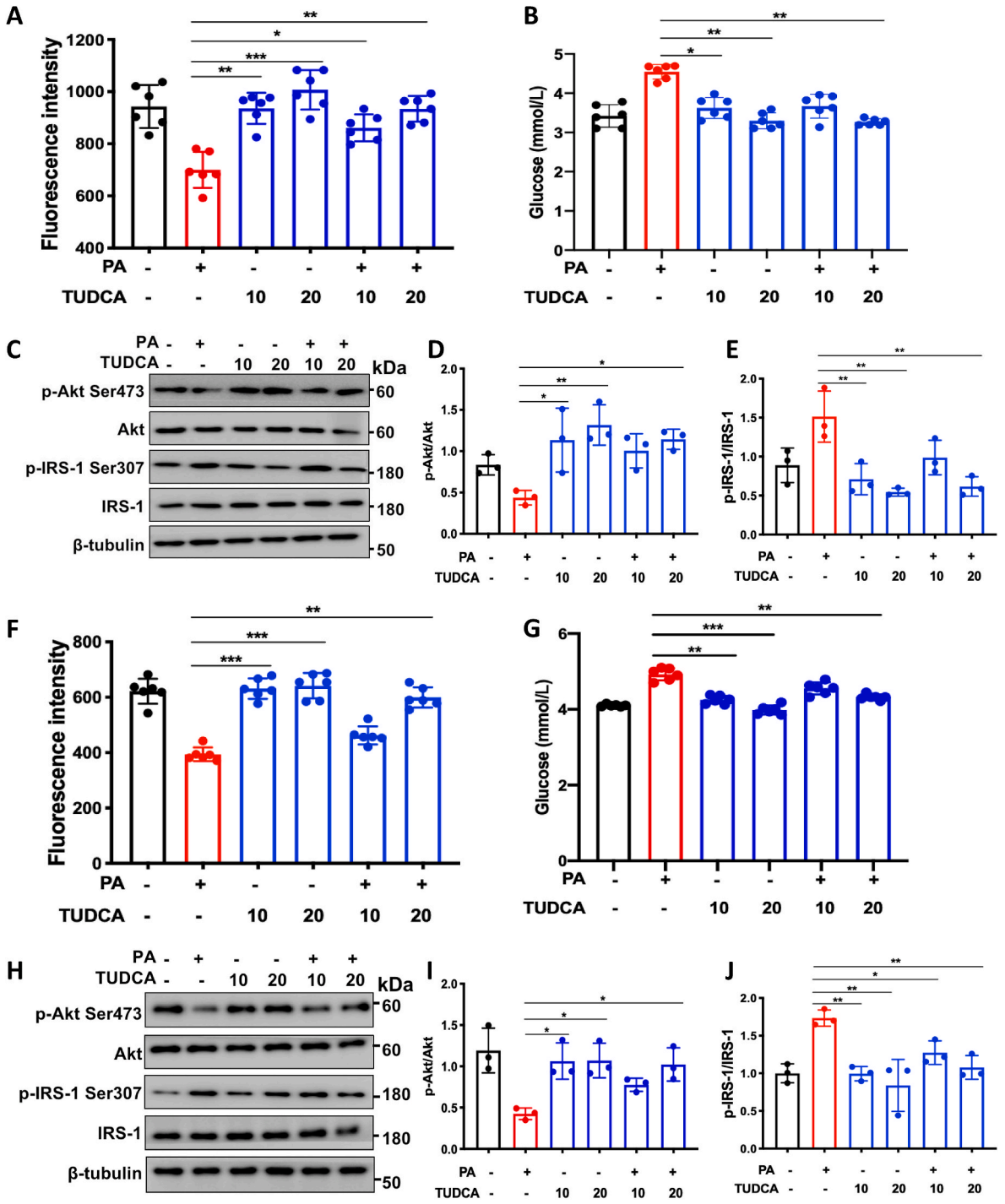

Fig. 3. TUDCA alleviates insulin resistance in PA-treated hepatocytes. (A–C) HepG2 cells were pre-treated with 200 μM PA for 24 h and then incubated with TUDCA (10 or 20 μM) for 12 h. (A) Glucose uptake and (B) glucose in the medium supernatant. (C) Protein levels of p-Akt, Akt, p-IRS-1, IRS-1 and quantitative analysis for (D) p-Akt and (E) p-IRS-1. (F–J) Primary mouse hepatocytes were pre-treated with 200 μM PA for 24 h and then incubated with TUDCA (10 or 20 μM) for 4 h. (F) Glucose uptake and (G) glucose in the medium supernatant. (H) Protein levels of p-Akt, Akt, p-IRS-1, IRS-1 and quantitative analysis for (I) p-Akt and (J) p-IRS-1. Results from three independent experiments are expressed as the mean ± SD. $^{*}P < 0.05$, $^{**}P < 0.01$ and $^{***}P < 0.001$. PA, palmitic acid; TUDCA, tauroursodeoxycholic acid.

Bacteroidetes ratio, the difference between the HFD group and the HFD + Met group is mainly reflected in the abundance reduction of Firmicutes and the increase in the abundance of Bacteroidetes (Fig. S7E). Among all the three groups, the HFD group had the highest levels of Erysipelotrichia and Bifidobacteriales, whereas HFD + Met group had the highest levels of Muribaculaceae, Tannerellaceae and *Parabacteroides* (Fig. S7E). Bile salt hydrolase (BSH) secreted by *Bifidobacterium* degrades the conjugated bile acids, such as TUDCA. Analysis of strains in *Bifidobacterium* revealed that the relative abundance of *B. pseudocatenulatum* and *B. choerinum* was significantly upregulated by HFD, which was dramatically diminished in the presence of metformin (Fig. 6C). Both content (Fig. 6D) and activity (Fig. 6E) of BSH were also decreased in the presence of metformin. The abundance of *B. pseudocatenulatum* and *B. choerinum* was negatively correlated with

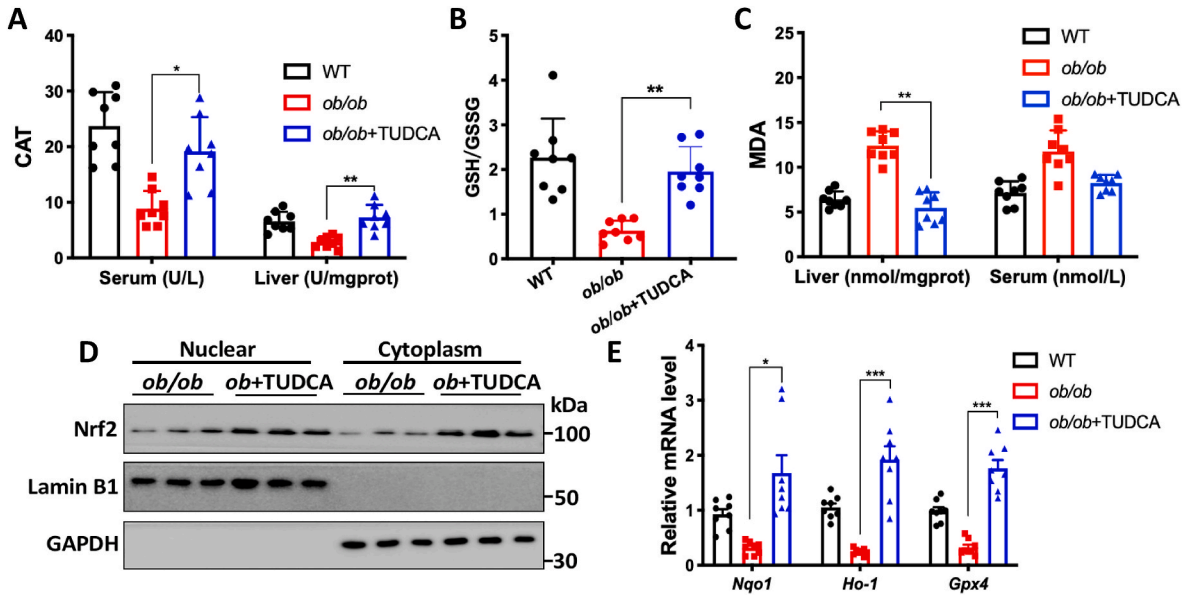

Fig. 4. TUDCA ameliorates oxidative stress in *ob/ob* mice. (A–C) Serum or liver homogenate were used to quantify the representative of oxidative stress: (A) CAT, (B) GSH:GSSG ratio, and (C) MDA. (D) Protein expression of Nrf2 in nuclear and cytoplasm. (E) Quantitative RT-PCR analysis of *Nqo1, Ho-1* and *Gpx4*. Data are expressed as mean ± SD. $^{*}P < 0.05$, $^{**}P < 0.01$ and $^{***}P < 0.001$ for HFD *vs* HFD + Met (n = 8). CAT, catalase; GSH, glutathione; GSSG, oxidized glutathione; MDA, malondialdehyde.

TUDCA content (Fig. 6F and G). By *in vitro* assay of enzymatic activity, we found that metformin did not directly inhibit the catalytic activity of BSH (Fig. 6H), suggesting that metformin induced accumulation of TUDCA is probably through gut microbiota remodeling and reduction of BSH.

2.6. *TUDCA promotes the proliferation of **Akkermansia muciniphila** and alleviated HFD-induced intestinal inflammation*

Gut microbiota and intestinal inflammation are closely related to IR. *Akkermansia muciniphila* helps alleviate features of metabolic syndrome in overweight and obese subjects. Fig. 7A and B suggested a correlation between intestinal metabolites and gut microbiome at the phylum and species levels, respectively. TUDCA was highly associated with *A. muciniphila* that belongs to the Verrucomicrobia phylum. Interestingly, the analysis of growth curves suggested that TUDCA rather than metformin accelerated the proliferation of *A. muciniphila in vitro* (Fig. 7C and D). In addition, in the presence of TUDCA, the abundance of *A. muciniphila* was significantly increased in *ob/ob* mice (Fig. 7E). The release and gene expression of pro-inflammatory factors (*Il-1β, Il-6,* and *Tnf-α*) in ileum were also decreased with TUDCA (Fig. 7F and G). Our data suggested that in addition to improving hepatic oxidative stress, TUDCA upregulates the intestinal abundance of *A. muciniphila,* alleviates intestinal inflammation and improves IR in obese mice.

3. Discussion

Metabolic dysfunction including obesity, NAFLD and T2DM are prevalent in the world today [2]. Metformin, as an anti-diabetic drug, facilitates cellular metabolism and thus alleviates IR [15]. Metabolic disease is also strongly correlated with gut microbiota [16] and bile acids [17]. Metformin impacts gut microbiota, bile acids and related host targets that mediate glucose metabolism [18,19]. We therefore investigated potential novel mechanisms of metformin in insulin sensitization through gut microbiota and intestinal metabolites. TUDCA was increased in both intestine and liver following treatment of metformin in obese models. TUDCA directly alleviated IR, reduced oxidative stress and intestinal inflammation in *ob/ob* mice. In the liver, TUDCA prevented KEAP1 binding with Nrf2 and thus activated the Nrf2/ARE signaling pathway. Nrf2 is important to ameliorate hepatic IR by reducing oxidative stress. Accumulation of TUDCA was associated with the effects of metformin on reducing the relative abundance of *Bifidobacteria* which is responsible for the production of BSH. In addition, TUDCA mitigated HFD-induced intestinal inflammation and increased the abundance of *A. muciniphila*.

TUDCA improves insulin sensitivity and increases pancreatic β cell mass in obese humans or murine models of obesity and diabetes [20,21]. TUDCA can mitigate endoplasmic reticulum (ER) stress and restore the expression of unfolded protein response (UPR) mediators [22], and is involved in PI3K/AKT cascade signaling activation to inhibit apoptosis [23,24]. Both effects in turn reduce apoptosis of pancreatic β cells and maintain insulin secretion [25]. TUDCA may also interact with membrane-bound bile acid receptors e.g. TGR5, and nuclear receptors e.g. FXR, both of which regulate metabolisms of glucose and lipids and control bile acid transportation and turnover [26,27]. In addition, TUDCA reduces cell mortality by reducing oxidative stress independent of ER stress [28]. A report also indicated that TUDCA reduced α-synuclein-induced oxidative stress in SH-SY5Y cells by increasing the expression of glutathione peroxidase (GPX) and hemeoxygenase-1 (HO-1) [29]. These findings together suggest that TUDCA has potential therapeutic effects on metabolic diseases.

Accumulating evidence has indicated that oxidative stress (such as mitochondrial dysfunction, ROS overproduction, and lipid peroxidation) plays an essential role in the pathological process of IR and impairs glucose tolerance in T2DM [30,31]. KEAP1-Nrf2 system prevents the development of IR [32]. We found that TUDCA antagonizes the binding between KEAP1 and Nrf2, and thus prevents Nrf2 degradation to activate the Nrf2/ARE signaling pathway. The up-regulation of Nrf2 through its genetic manipulation and pharmacological interference significantly reduces the content of ROS and ameliorates IR and T2DM [32–35]. In the presence of metformin, the up-regulation of *Nrf2* expression and its downstream target genes (*Gclc*, *Cat* and *Ho-1*) alleviate IR and oxidative stress [36,37]. Conversely, the stress-resistant effect of TUDCA was dramatically repressed by the inhibition of the Nrf2/ARE signaling. We also found that TUDCA can effectively reduce inflammation and oxidative stress as well as the accumulation of lipid peroxide *in vitro* and *in vivo*, suggesting that TUDCA is a potential lead compound for the treatment of IR and diabetes.

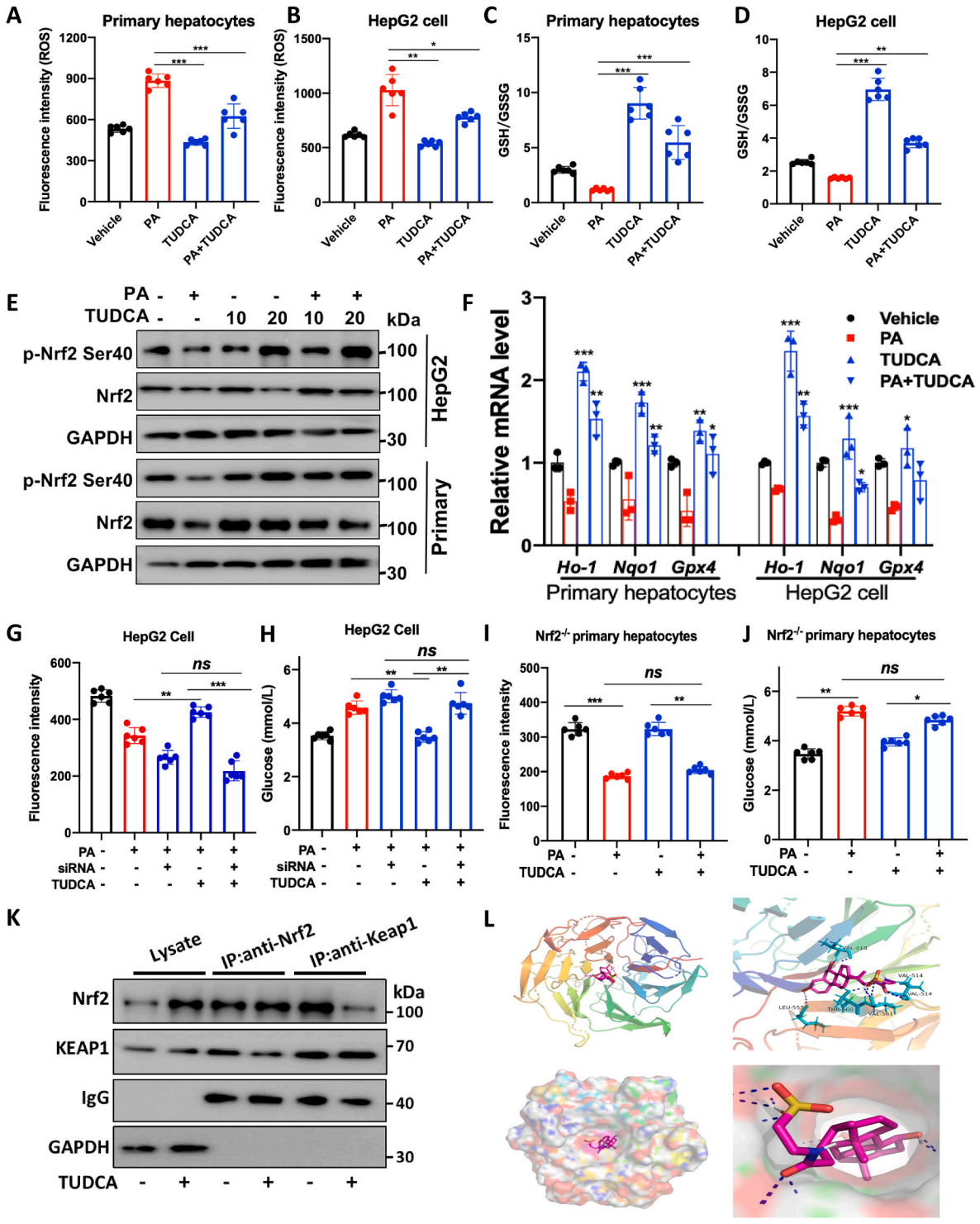

Fig. 5. TUDCA relieves PA-induced insulin resistance *via* activating Nrf2/ARE signaling pathway. The content of ROS in (A) primary hepatocytes and (B) HepG2 cells. The ratio of GSH/GSSG in (C) primary hepatocytes and (D) HepG2 cells. (E) Protein levels of p-Nrf2 and Nrf2 were determined by western blotting in primary mouse hepatocytes and HepG2 cells. (F) Quantitative RT-PCR analysis of *Nrf2*, *Ho-1*, *Nqo1* and *Gpx4* in primary mouse hepatocytes and HepG2 cells. (G) Glucose uptake by cells and (H) glucose content of the medium supernatant measured in Nrf2 knock-down HepG2 cells. (I) Glucose uptake by cells and (J) glucose content of the medium supernatant were measured in primary hepatocytes from Nrf2$^{-/-}$ mice. (K) Immunoprecipitation. HepG2 cells were treated with or without TUDCA (20 μM), and then lysates were immunoprecipitated with the indicated antibodies, followed by western blotting. (L) Docking of TUDCA with Kelch domain of KEAP1. The residues of KEAP1 were represented using sticks or surface structures, TUDCA was shown in pink, the dashed lines (blue) represent hydrogen-bonding interactions. Results from three independent experiments are expressed as mean ± SD. *$P < 0.05$, **$P < 0.01$ and ***$P < 0.001$. ROS, reactive oxygen species; GSH, glutathione; GSSG, oxidized glutathione; PA, palmitic acid; TUDCA, tauroursodeoxycholic acid. (For interpretation of the references to color in this figure legend, the reader is referred to the Web version of this article.)

Table 1
Diversity of gut microbiota in HFD and HFD + Met treated mice.

Groups	Reads	OTUs	Observed species	Ace	Chao1	Shannon	Simpson
NCD	78316 ± 4945	372 ± 35	330 ± 21	345 ± 17	350 ± 21	5.10 ± 0.67	0.92 ± 0.04
HFD	76154 ± 7745	350 ± 40	312 ± 20	325 ± 24	326 ± 24	5.38 ± 0.33	0.95 ± 0.02
HFD + Met	80004 ± 421	374 ± 21	335 ± 20*	342 ± 22*	348 ± 20*	5.24 ± 0.27	0.95 ± 0.02

Data are expressed as mean ± SD. *$P < 0.05$ compared with HFD, n = 6. OTUs, operational taxonomic unit; NCD, normal chow diet; HFD. high fat diet; Met, metformin.

The "dialogue" between the gut microbiota and the organism mainly depends on microbial metabolites. By producing various enzymes for biochemical metabolic pathways of the intestinal microbes, gut microbiota performs diverse metabolic activities such as the metabolism of amino acids, carbohydrates and bile acids, as well as establishes a co-metabolic relationship with the host [38]. A portion of TUDCA is derived from the conversion of taurochenodeoxycholic acid (TCDCA) in the colon, which is catalyzed by 7α/β-hydroxysteroid dehydrogenase (7α/β-HSDH) that is mainly produced by two genera of intestinal bacteria, *Eubacterium* and *Clostridium* [39,40]. Our data from the 16S rRNA amplicon sequencing show that metformin does not affect the abundance of *Eubacterium* and *Clostridium*. The levels of conjugated bile acid TUDCA in the gut are also influenced by bile salt hydrolase (BSH). Intestinal bacteria, especially *Bifidobacterium*, produce BSH, which hydrolyse TUDCA to taurine and ursodeoxycholic acid (UDCA). Consistent with our present findings, metformin treatment could increase the amount of secondary bile acids (e.g., TUDCA, UDCA, and GUDCA) in the feces of mice on a high-fat/sucrose diet by modifying the gut microbiota (e.g., *Lachnospiraceae*, *Clostidium*, *Bacteroides*, etc.) [14,41]. In addition, our results showed that metformin cannot directly inhibit the catalytic activity of BSH of intestinal bacteria isolated from mouse feces (Fig. 6H). Therefore, it is speculated that the TUDCA accumulation is probably due to a reduction in BSH-producing bacteria *B. pseudocatenulatum* and *B. choerinum* since metformin reshaped the gut microbiota. This presumption is strongly supported by a recently conducted clinical study in Indonesian [42]. The researchers systematically analyzed the fecal microbiota and metabolites of 75 Indonesian adults in Yogyakarta City, including obese individuals, T2DM patients, and healthy individuals, together with their dietary and medical records. This study found that HFD-driven Indonesian obesity is associated with the dysbiosis of gut microbiota with the reduction of intestinal secondary bile acids. Notably, T2DM in the Indonesian subjects is associated with an increased abundance of Bacteroides equipped with strong BSH activity, as well as the loss of conjugated bile acids particularly TUDCA, while these alterations are reversed in patients receiving metformin treatment. In addition, another study found that metformin simultaneously upregulates the levels of two conjugated bile acids, GUDCA and TUDCA, and the former acts as an inhibitor of the hepatic FXR signaling to alleviate metabolic dysfunction [14]. However, it should be noted that our present study did not identify the differences in GUDCA between the HFD group and the metformin-treated group using non-targeted metabolomic analysis, which may be due to the limitation of the sensitivity of this technique or to the low abundance of GUDCA itself. While the above mentioned studies only observed that metformin administration elevated the intestinal TUDCA levels and it is still unconfirmed that whether metformin alleviated insulin resistance *via* TUDCA in patients with diabetes, a clinical investigation provides direct evidence that TUDCA alleviates insulin resistance in obese patients [20]. In this study, 20 obese individuals were randomized to 4 weeks of treatment with or without TUDCA (1,750 mg/day). The researcher found that hepatic and muscle insulin sensitivity increased by approximately 30% after treatment with TUDCA, as well as the increased muscle insulin signaling (p-IRS-1 and p-Akt at Ser473 levels), which greatly supports our present findings. The proportion of TUDCA in the bile acid pool is very low, thus the physiological and pharmacological activities of TUDCA are often neglected. Through the above studies, it is well demonstrated that metformin remodels the gut microbiota, reduces oxidative stress and enhances insulin sensitivity partly due to increasing the levels of TUDCA, which functions as an important mediator for metformin's pharmacological activities.

In terms of the beneficial microbes identified, *A. muciniphila* colonizes the mucosa layer of the intestine and modulates basal metabolism. *A. muciniphila* is prospective for alleviating intestinal inflammation and metabolic disorders associated with obesity, which has been proved by a variety of animal models and human studies, thus transplanting *A. muciniphila* has been considered for next-generation therapeutic strategy for metabolic syndrome [43,44]. The abundance of *A. muciniphila* was significantly reduced in obese individuals compared with healthy people [45]. Numerous studies have demonstrated that metformin could up-regulate the abundance of *A. muciniphila* in HFD-fed mice, maintain intestinal integrity as well as effectively ameliorate intestinal inflammation [46,47]. These functions further leads to a decrease in serum LPS and the amelioration of systemic inflammation and IR in obese individuals. Notably, the present data demonstrated that metformin does not significantly accelerate the proliferation of *A. muciniphila in vitro*, but TUDCA does (Fig. 7D). Consistent with these findings, TUDCA treatment significantly increased the abundance of *A. muciniphila* in *ob/ob* mice (Fig. 7E). Similarly, we found that TUDCA administration by gavage for one week increased the abundance of *A. muciniphila* in wild-type C57BL/6 mice (data not shown). Therefore, we speculate that metformin increased the abundance of *A. muciniphila* in HFD-fed mice, probably due to upregulating TUDCA content *via* metformin administration. The potential mechanism of how TUDCA accelerates the proliferation of *A. muciniphila* will be explored in our future studies.

Overall, in our present study, metformin was demonstrated to significantly increase the accumulation of TUDCA possibly by remodeling gut microbiota, reducing the abundance of *B. pseudocatenulatum* and *B. choerinum* as well as the production and activity of BSH. TUDCA antagonized the interaction between KEAP1 and Nrf2, prevented Nrf2 degradation and promoted its nuclear translocation and transcription initiation of the antioxidant genes, thereby reducing oxidative stress and improving insulin signaling. Moreover, TUDCA promotes the proliferation of *A. muciniphlia in vitro* and *in vivo,* which maintains intestinal integrity and reduced inflammation in obese mice. We here revealed that metformin remodels the gut microbiota, reduces oxidative stress and enhances insulin sensitivity partly due to increasing the accumulation of TUDCA. The present study provided a novel mechanism by which TUDCA functions as an essential mediator for metformin's insulin sensitization, and the study also appeals that TUDCA is a potential lead compound in alleviating metabolic syndrome.

4. Materials and methods

4.1. Chemicals and diet

Metformin (purity ≥98%), choline (purity ≥98%), taurine (purity ≥99%) and palmitic acid (PA, purity ≥99%) were obtained from Sigma-Aldrich (St. Louis, MO, USA). Tauroursodeoxycholic acid (TUDCA, purity ≥99%) was purchased from Selleck (Houston, Texas, USA). Both the normal chow diet (NCD, containing 10% fat by energy) and high-fat diet (HFD, containing 60% fat by energy) were purchased from Beijing HFK Bio-Technology Co., Ltd. (Beijing, China). Antibodies against Akt (#4691), phospho-Akt (Ser473, #4060), IRS-1 (#2390), phospho-IRS-1

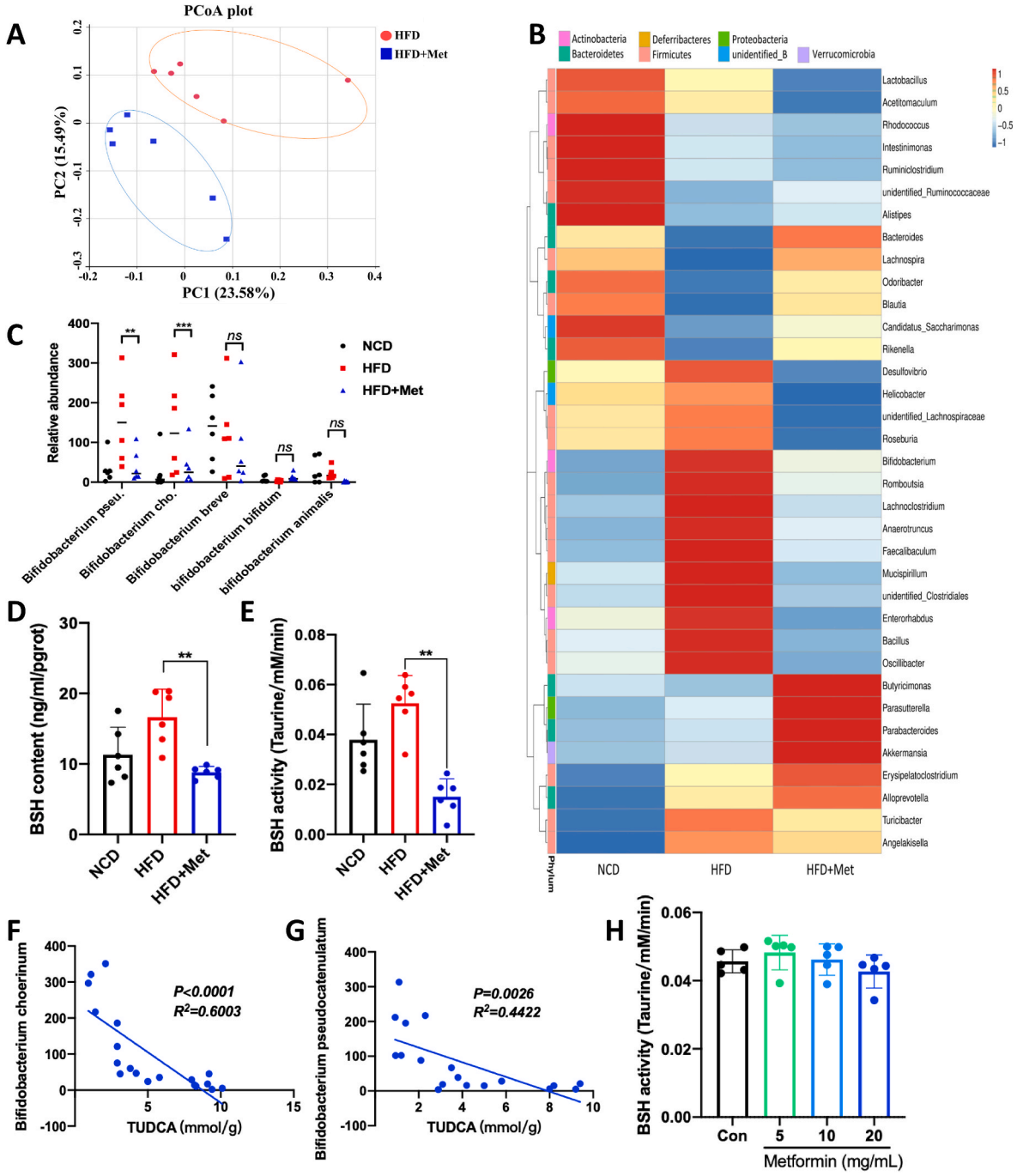

Fig. 6. Metformin increased TUDCA accumulation by decreasing the abundance of *Bifidobacterium* thus reducing BSH production. (A) Principal coordinates analysis. (B) Heatmap showing clustering of bacterial communities with their relative abundances at the genus level, the bacterial communities or OTUs were clustered phylogenetically by neighbor-joining method and the libraries were clustered by profile pattern using Unifrac analysis. Relative abundances (log values) of microbial genus are displayed in a red-to-blue color code (high to low abundance). (C) Relative abundance of different strains of *Bifidobacterium*. (D) BSH content and (E) BSH activity in mouse feces. Correlation analysis between TUDCA levels and the relative abundance of (F) *B. choerinum* and (G) *B. pseudocatenulatum*. (H) Fecal suspensions were prepared by collecting fresh feces, adding metformin to final concentrations of 5, 10 and 20 mg/mL, incubating for 30 min and then measuring BSH activity. Data are expressed as mean ± SD. $^{*}P < 0.05$, $^{**}P < 0.01$ and $^{***}P < 0.001$ for HFD *vs* HFD + Met (n = 6). PCoA, principal coordinates analysis; BSH, bile salt hydrolase. (For interpretation of the references to color in this figure legend, the reader is referred to the Web version of this article.)

(Ser307, #2381), KEAP1 (#8047), GAPDH (#5174), lamin B1 (#13435) and β-tubulin (#2128) were obtained from Cell Signaling Technology (Beverly, MA, USA). Nrf2 (ab62352), phospho-Nrf2 (Ser40, ab76026), IgG (ab181236) and 4-HNE (ab46545) were purchased from Abcam (Cambridge, UK). Horseradish peroxidase (HRP)–conjugated secondary antibody was obtained from Santa Cruz Biotechnology (Santa Cruz, USA).

4.2. Animal experiments

All male mice (ICR mice, 7 weeks old, body weight 25 ± 2 g; C57BL/6J mice, 7 weeks old, body weight 20 ± 2 g; *ob/ob* mice, 7 weeks old, body weight 40 ± 2 g; $Nrf2^{-/-}$ mice, 7 weeks old, body weight 20 ± 2 g) were housed in ventilated cages (three animals per cage) at the SPF facility of Wenzhou University under controlled environmental

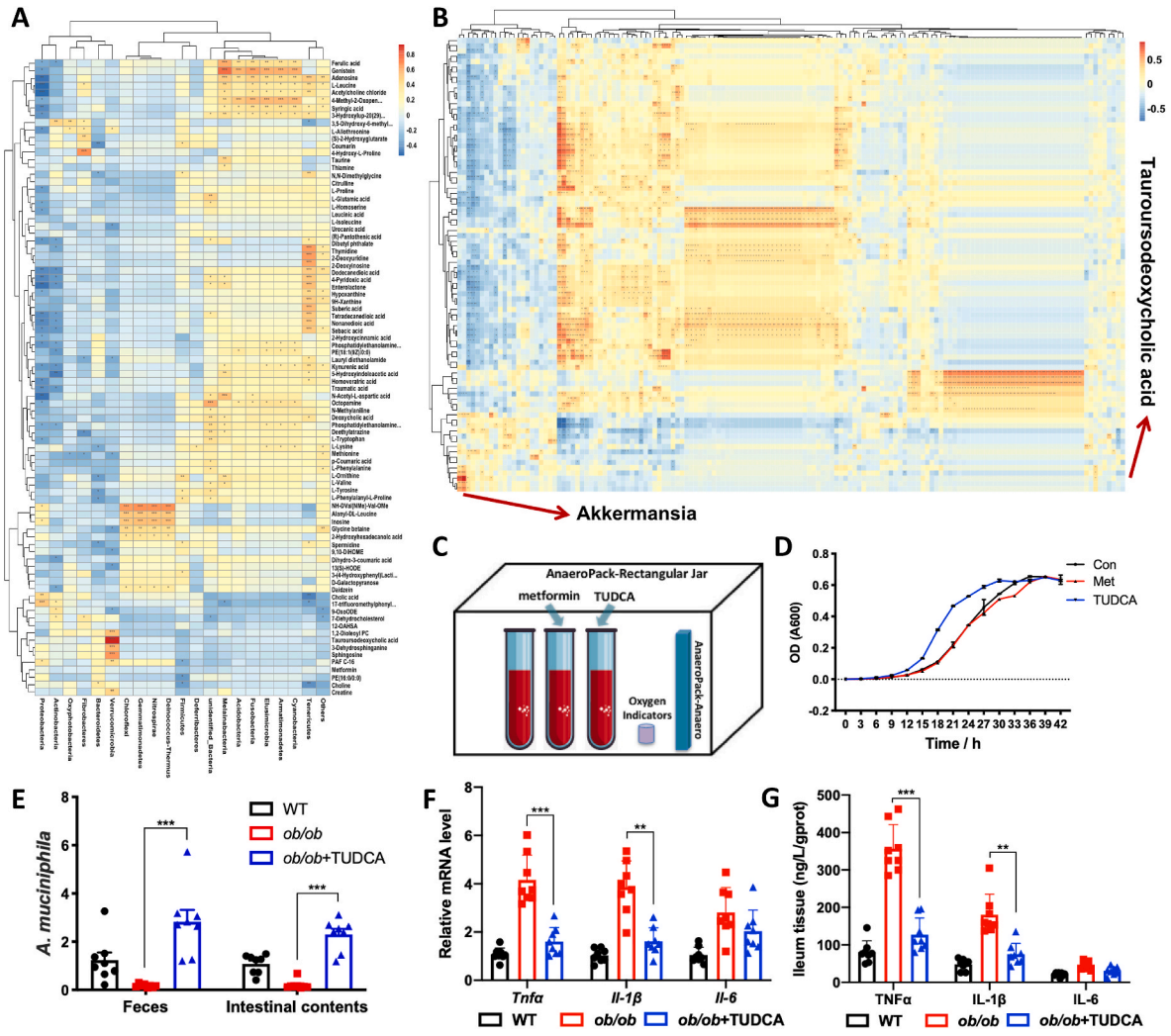

Fig. 7. Correlation heatmap for gut microbiota and differential metabolites. (A–B) The correlation coefficients of the gut microbiota and differential metabolites were calculated by Pearson's algorithm using the R language, and heatmaps were created based on the correlation coefficients. Matrix heatmap showing the correlation between gut microbiota and differential metabolites at (A) phylum and (B) species levels, respectively. (C) The schematic diagram of the anaerobic device and (D) growth curve of *A. muciniphila* in the presence of metformin or TUDCA. (E) Abundance of *A. muciniphila*. The expression of pro-inflammatory cytokines in the ileum were determined at (F) protein level and (G) mRNA level. Data are expressed as mean ± SD. $^{*}P < 0.05$, $^{**}P < 0.01$ and $^{***}P < 0.001$ for *ob/ob* vs *ob/ob* + TUDCA (n = 8).

conditions (temperature 22 ± 2°C; relative humidity 60–70%) with free access to standard laboratory chow and tap water. The mice were maintained on a regular 12/12 h light/dark cycle.

All mice were acclimatized to their environment for 1 week before the experiments. The schematic of animal experimental design was shown in Fig. 1A. A co-worker blinded to the experimental protocol randomized animals into these groups (n = 9 for each group). As for the pharmacological activity of metformin, one group of ICR mice was fed with NCD (10 kcal% fat) and the other two groups were fed with HFD (60 kcal% fat, the compositions included 68.5% AIN-93 diet, 20% lard oil, 10% egg yolk powder, 1% cholesterol, and 0.5% sodium cholate.). After 12 weeks of HFD feeding, one group of HFD-fed mice was administered metformin (200 mg/kg body weight), once daily (HFD + Met group) for 8 weeks, whereas the NCD-fed mice (NCD group) and another group of HFD-fed mice (HFD group) were treated with an equal volume of saline for 8 weeks. The whole study lasted 20 weeks, during which the body weight, water consumption and food intake were measured every week. At week 19, the intraperitoneal glucose tolerance test (IPGTT) and intraperitoneal insulin tolerance test (IPITT) were performed as previously described [1]. As for the pharmacological activity of TUDCA, one group of *ob/ob* mice was administered TUDCA (300 mg/kg body weight), whereas the wild-type C57BL/6J mice and *ob/ob* mice in the other two groups were treated with an equal volume of saline for 8 weeks as control.

At the end of the trial, after overnight fasting for 12 h, blood samples were collected, and serum was isolated by centrifugation at 1000 × *g* for 15 min at 4°C, and stored for further assay. Tissues, including the adipose tissue, liver and ileum, were weighed; one portion of the tissues was fixed with 10% formaldehyde for histological analysis, and the other portion was immediately frozen in liquid nitrogen for further analysis.

Organ indexes were calculated by the following formula:

$$\text{BMI} = \text{body weight (kg)/body length (m)}^2$$

$$\text{Liver index} = \text{wet weight of liver/BW* 100\%}$$

$$\text{Kidney index} = \text{wet weight of kidney/BW* 100\%}$$

$$\text{Pancreas index} = \text{wet weight of pancreas/BW* 100\%}$$

$$\text{Subcutaneous fat index} = \text{wet weight of adipose tissue/BW * 100\%}$$

4.3. Biochemical analysis

Total cholesterol (T-CHO), triacylglycerol (TG), free fatty acids (FFA), fasting blood glucose (FBG), fasting serum insulin (FINS), acid phosphatase (ACP), alkaline phosphatase (AKP), alanine aminotransferase (ALT), aspartate aminotransferase (AST), catalase (CAT), malondialdehyde (MDA), lipopolysaccharides (LPS) were determined by biochemical kits purchased from Jiancheng Bioengineering Institute (Nanjing, China). The bile salt hydrolase (BSH) content was determined by a biochemical kit purchased from Jianglia Bioengineering Institute (Shanghai, China). The ratio of reduced glutathione (GSH) and oxidized glutathione (GSSG) was determined by a GSH:GSSG kit (Jiancheng Bioengineering Institute, Nanjing, China). Homeostasis model assessment-estimated insulin resistance (HOMA-IR) was calculated using the following formula:

$$\text{HOMA-IR} = \text{FBG (mmol/L)} \times \text{FINS (mU)}/22.5$$

4.4. Hematoxylin and eosin staining

Adipose tissue was fixed in 10% formaldehyde overnight, paraffin-embedded, sectioned (4-μm thickness, 3–5 sections/specimen) and stained with hematoxylin and eosin (H&E) for histological analysis. Digital images of H&E stained sections were acquired with a Nikon Eclipse Ti microscope at × 400 magnifications (Ti-E/U/S, Japan). Image J software (National Institutes of Health, USA) was used to count adipocytes.

4.5. Cell culture

Human liver hepatocellular carcinoma (HepG2) cells were cultured in MEM (Sigma, St. Louis, MO, USA) supplemented with 10% FBS, penicillin and streptomycin. Cells were maintained in 5% CO_2 at 37°C.

4.6. Isolation and culture of primary hepatocytes

Male C57/B6J and Nrf2$^{-/-}$ mice (8 weeks old) were used for isolating primary hepatocytes. Hepatocytes were isolated by a two-step collagenase perfusion technique. Briefly, the inferior vena cava was cannulated with angiocatheter and the portal vein was cut. The liver was perfused *via* the inferior vena cava with 100 mL of PBS at 37°C, followed by perfusion with 100 mL of collagenase type IV (Wellington) in HBSS containing Ca^{2+} and Mg^{2+} (GIBCO). After the liver was digested, it was dissected and cut into small pieces and passed through a 100 μm strainer (Falcon). Hepatocytes were separated from non-parenchymal cells by low-speed centrifugation and further purified by Percoll gradient centrifugation (50% v/v, Sigma). Cells were plated at a density of 0.3 × 10^6 on a 6-well collagen-coated plate. Hepatocytes were allowed to recover overnight and experiments were started 24 h post isolation.

4.7. siRNA transfection

Nrf2 was knocked down by RNA interference (RNAi) using the following 19-bp (including a 2-deoxynucleotide overhang) siRNAs (Origene, Beijing, China): *Nrf2*, SR321100A-AUUGAUGUUUCUGAUCU AUCACUTT; SR321100B-GUCAGUAUGUUGAAUCAGUAGUUTC; SR32 1100C-CCAGUCUUCAUUGCUACUAAUCAGG. Stealth RNAi (Origene, Beijing, China) was used as a negative control (siCont). For transfection, cells were seeded on a six-well plate, grown to ~80% confluence and transfected with siRNA duplexes using Lipofectamine 3000 (Invitrogen, Camarillo, CA, USA) according to the manufacturer's recommendations. After incubation for 48 h, the expression level of Nrf2 protein was detected by western blotting.

4.8. Glucose uptake assay

Cells were plated at 1 × 10^4/well in 96-well plates and used at subconfluence after 24 h of preincubation. For experiments, all culture medium was removed from each well and replaced with 100 μM fluorescent 2-Deoxy-2-[(7-nitro-2,1,3-benzoxadiazol-4-yl) amino]-D-glucose (2-NBDG) in serum-free medium and incubated for 30 min. Subsequently, cells were washed thrice with PBS and then the fluorescence intensity was determined with a fluorescence microplate reader (Ex/Em, 488/520 nm). The glucose concentration in the medium supernatant was determined by a glucose detection kit (Jiancheng Bioengineering Institute, Nanjing, China).

4.9. Determination of ROS levels

Intercellular ROS levels were measured using a ROS Assay Kit (Beyotime, Shanghai, China) according to the manufacturer's protocol. In brief, the dichlorodihydrofluorescein diacetate (DCFH-DA; 10 mM) supplied in the kit was diluted to 10 μM in a serum-free medium. Subsequently, cells were pretreated with TUDCA (20 μM) for 2 h at a density of 3 × 10^3/96-well. Next, 200 μM PA solution was added and co-incubated for 24 h. The supernatant was then replaced with a serum-free medium. The DCFH-DA solution (10 μM) was added to the cells for 30 min at 37°C, and they were then resuspended with PBS (0.1 mM) after washing twice with the indicated inducers. Fluorescence intensity was detected using a hybrid/multi-modereaders (BioTek Instruments Inc., Vermont, USA) to determine ROS levels.

4.10. Quantitative RT-PCR

Total mRNA was isolated from tissue samples using TRIzol reagent (TAKARA, Tokyo, Japan) and was reverse-transcribed into cDNA using a high-capacity cDNA reverse transcription kit (TAKARA, Tokyo, Japan) according to the manufacturer's protocol. The mRNA levels were quantified with quantitative PCR (qPCR) using SYBR Green (Qiagen, Hilden, Germany). Amplification was performed on a LightCycler480 *q*RT-PCR system (Roche, Mannheim, Germany) under the following reactions: 95°C for 15 min, followed by 40 cycles at 95°C for 10 s, 60°C for 20 s, and 72°C for 20 s. The relative mRNA levels of target genes were normalized to the expression of β-actin calculated using the $2^{-\Delta\Delta ct}$ method. The primer pairs used in this study are listed in Supplementary Table 1.

4.11. Western blotting

Samples were homogenized with ice-cold RIPA lysis buffer containing protease and phosphatase inhibitors (Beyotime, Shanghai, China). The homogenates were centrifuged at 10 000 × *g* for 20 min at 4°C to remove the insoluble tissue debris. The protein concentration in the supernatant was determined using a BCA protein assay kit (Beyotime, Shanghai, China). Equal amounts of protein for each group were denatured in boiling water for 5 min. Aliquots (40 μg) of protein samples were subjected to 10% SDS-PAGE and transferred to PVDF membranes (Millipore, Bedford, MA, USA). After blocking with 5% nonfat milk (dissolved in TBST) for 1 h, the membranes were incubated with the indicated antibodies at 4°C overnight, followed by incubation with the appropriate HRP-conjugated second antibodies for 1 h at room temperature. Chemiluminescent detection was performed using the ECL Plus Western blotting reagent (TransStart, Beijing, China). Semi-quantitative analysis for densitometry of each band was performed using ImageJ software.

4.12. Co-immunoprecipitation

For co-immunoprecipitation (Co-IP), the whole protein lysates prepared from HepG2 cells were extracted in a RIPA lysis buffer. Briefly,

cell lysates were incubated with Nrf2 or KEAP1 antibodies for 2 h at room temperature, followed by binding of antigen antibody complexes to protein A/G magnetic beads (Thermo Scientific. Rockford, USA) for 1 h. Then, the antigen/antibody immunocomplex was stripped by boiling with a 5 × loading sample buffer for western blotting incubated with KEAP1, Nrf2 and GAPDH antibodies.

4.13. Methodologies of gut microbiota by 16S rRNA amplicon sequencing

Sample preparation: Fæcal samples were freshly collected at week 16 and immediately stored at −80°C. Total fecal DNA was extracted using CTAB/SDS method. The V4 region of the 16S rRNA was amplified using the universal primers 515F and 806R. All PCR reactions were carried out with Phusion® High-Fidelity PCR Master Mix (New England Biolabs), and the mixture PCR products were purified with GeneJET Gel Extraction Kit (Thermo Scientific). Sequencing libraries were generated using Ion Plus Fragment Library Kit (Thermo Scientific) following manufacturer's recommendations. The library quality was assessed on the Qubit 2.0 Fluorometer (Thermo Scientific). At last, the library was sequenced on an Ion S5™ XL platform (Thermo Scientific) and 400 bp/600 bp single end reads were generated. Sequence analysis was performed by Uparse software (v7.0.1001), and Sequences with ≥97% identity were assigned to the same Operational Taxonomic Units (OTUs). The detailed information on sample sequencing was shown in Supplementary Table 2.

Data analysis: To compare the compositional OTUs of the gut microbiota in each group, a Venn diagram was constructed using R packages (version 3.1.0) as previously documented. Mothur software packages (version V.1.30.1) were used to calculate the value of Chao1, Ace, Simpson index and Shannon index for evaluation of the community richness and community diversity. Pair-group method with arithmetic means (UPGMA) clustering was generated using the average linkage and conducted by QIIME software (V1.7.0). Linear discriminant analysis (LDA) was carried out to determine the highly dimensional gut microbes and characteristics associated with NCD mice, HFD mice and HFD + Met mice.

4.14. Methodologies of non-targeted metabolome analysis

Metabolite extraction from colon contents: Colon contents were added ddH2O (4°C) and mixed. 100 mg of sample was extracted with 1000 μL of pre-cooled methanol (−20°C). After centrifugation, the supernatant was evaporated and finally dissolved in 400 μL methanol aqueous solution (1:1, 4°C). For the quality control (QC) samples, 20 μL of extract was taken from each sample and mixed. These QC samples were used to monitor deviations of the analytical results from these pool mixtures and compare them to the errors caused by the analytical instrument itself. And the rest of the samples were used for LC-MS detection.

UPLC Conditions: Chromatographic separation was accomplished in an Acquity UPLC system equipped with an ACQUITY UPLC® HSS T3 (150 × 2.1 mm, 1.8 μm, Waters) column maintained at 4°C. The temperature of the auto sampler was 4°C. Gradient elution of analytes was carried out with 0.1% formic acid in water (A) and 0.1% formic acid in acetonitrile (B) at a flow rate of 0.25 mL/min. Injection of 5 μL of each sample was done after equilibration. An increasing linear gradient of solvent B (v/v) was used as follows: 0–1 min, 2% B; 1–9.5 min, 2%~50% B; 9.5–14 min, 50%~98% B; 14–15 min, 98% B; 15–15.5 min, 98%~2% B; 15.5–17 min, 2%.

Mass spectrometry conditions: The ESI-MS^n experiments were executed on the Thermo LTQ Orbitrap XL mass spectrometer with the spray voltage of 4.8 kV and −4.5 kV in positive and negative modes, respectively. Sheath gas and auxiliary gas were set at 45 and 15 arbitrary units, respectively. The capillary temperature was 325°C. The voltages of capillary and tube were 35 V and 50 V, −15 V and −50 V in positive and negative modes, respectively. The Orbitrap analyzer scanned over a mass range of *m/z* 89–1000 for full scan at a mass resolution of 60000. Data dependent acquisition (DDA) MS/MS experiments were performed with CID scan. The normalized collision energy was 30 eV. Dynamic exclusion was implemented with a repeat count of 2, and exclusion duration of 15 s.

Data processing: UPLC-QTOF-MS raw data were analyzed with MarkerLynx Application Manager 4.1 (Waters Corp.). The matrix from UPLC-QTOF-MS was introduced into SIMCA-P 11.0 software (Umetrics) and standardized to a mean of 0 and variance of 1, according to the formula [X - mean(X)]/std (X), for multivariate statistical analysis. The *t*-test with false discovery rate correction was used to measure the significance of each metabolite. Partial least-squared discriminant analysis (PLS-DA) and orthogonal partial least-squared discriminant analysis (OPLS-DA) were conducted to identify the metabolite discrimination between the two group samples. Differential metabolites were defined with variable importance in the projection (VIP) > 1.0 obtained from OPLS-DA and *P* values less than 0.05 obtained from *t*-test. Differential metabolites were tentatively identified by database matching, i.e., Human Metabolome Database (HMDB) (http://www.hmdb.ca), Metlin (http://metlin.scripps.edu), massbank (http://www.massbank.jp/), LipidMaps (http://www.lipidmaps.org), mzclound (https://www.mzcloud.org). Heatmaps of differential metabolites among all groups were obtained based on spearman correlation and cluster analyses.

4.15. Growth curve of Akkermansia muciniphila

Akkermansia muciniphila strain ATCC BAA-835 was purchased from the Beina Biologicals, Inc. (Beijing, China). Bacteria were cultured in BHI medium in tubes at 37°C in an anaerobic chamber (Whitley A35 Workstation 2.5, Don Whitley Scientific, UK). To acquire the growth curve of *A. muciniphila*, the medium in test tubes supplemented with or without 10 mM metformin (or 20 μM TUDCA) was placed in an anaerobic bag to eliminate oxygen for 24 h. The test tubes were then inoculated with bacteria and incubated at 37°C in an anaerobic bag. The OD_{600} of the cultures was measured every 3 h.

4.16. Determination of hepatic/serum TUDCA

The contents of TUDCA in tissues were determined by high-performance liquid chromatography (HPLC). Briefly, 200 mg of frozen tissue was homogenized with a Qiagen TissueLyserII (Germantown, MD, USA) in 1 mL of PBS to prepare the tissue homogenates. The impurities were removed through a 0.22 μm filter, then the filtrate was precipitated by methanol and 10 μL of supernatant was analyzed using an Agilent 1290 HPLC system (Santa Clara, CA) equipped with a Hypersil ODS-2 column (5 μm, 4.6 × 250 mm; Waters, USA). The supernatant was detected at the wavelength of 210 nm, and eluted with the mobile phase of 0.03 M phosphate buffer solution (pH 4.4) and methanol (32:68, v/v) at a flow rate of 1.0 mL/min.

4.17. Determination of BSH activity in vitro

The enzyme activity of BSH was determined using an amino acid chromogenic method. Briefly, mouse feces were collected and the fecal suspension was prepared. 10 μL of sample (containing 500 μg of protein) was incubated with 180 μL of sodium phosphate buffer and 10 μL of TDCA (final concentration 10 mM) at 37°C for 30 min. 50 μL of the mixture was mixed with 50 μL of 15% TCA and centrifuged at 10,000g for 10 min. Mix 20 μL of supernatant with 80 μL of water, add 1.9 mL of ninhydrin (0.5 mL 1% ninhydrin, 1.2 mL glycerol, 0.2 mL 0.5 M citrate buffer, pH 5.5) and boil for 15 min. Cool the reaction tube, measure the absorbance at 570 nm and calculate the BSH enzyme activity by substituting the formula for the taurine standard curve.

4.18. Molecular docking analysis

To investigate the probable binding of TUDCA to KEAP1 as the potential inhibitor, the automated docking studies were carried out using AutoDock vina 1.1.2 package. The X-ray crystal structure of the human KEAP1 (PDB ID: 6LRZ) was downloaded from RCSB Protein Data Bank. The 3D structure of TUDCA (ZINC ID: 3914813) was downloaded from ZINC. The AutoDockTools 1.5.6 package was employed to generate the docking input files. The molecular docking simulation protein of Keap1 was prepared by removing water molecules and bound ligands. The binding site of the KEAP1 was identified as centre_x: −9.944, centre_y: −38.993, and centre_z: 3.869 with dimensions size_x: 85, size_y: 85, and size_z: 85. The best-scoring (i.e.,with the lowest docking energy) pose as judged by the Vina docking score was chosen and further analyzed using PyMoL 2.4.0 software.

5. Statistical analysis

Statistical analysis of the data collected (from various independent experiments) was performed using GraphPad Prism 8.0 software (GraphPad Software, Inc., La Jolla, CA, USA) and SPSS 20 Statistical Analysis Software (SPSS Inc., Chicago, IL, USA). The Shapiro–Wilk Test was used to test the normality of the data. All experimental results are presented as mean ± SD, and statistical significance was determined by one-way analysis of variance (ANOVA) followed by Tukey's test. The values were significantly different at $p < 0.05$.

Financial support

This work was financially supported by the National Natural Science Foundation of China (81872952 and 41876197), the Science and Technology Program of Wenzhou (ZY2019013).

Authors' contributions

Y.Z., J.L, Y.C., J.Z. and L.Y performed the research. H.T., Y.Z. and Y. G. designed this study. R.T. and M.W. provided technical assistance. H. T. and Y.Z. analyzed the data and wrote the manuscript. X.B. And D.Q. revised the manuscript. H.T. and Y.G. had primary responsibility for final content. All authors have read and approved the final manuscript.

Declaration of competing interest

The authors declare that they have no known competing financial interests or personal relationships that could have appeared to influence the work reported in this paper.

Data availability

Data will be made available on request.

Acknowledgements

We gratefully thank Qiaojuan Li and Lingfeng Hou (Wenzhou University) for their assistance in animal experiments. We gratefully thank Alan K Chang (Wenzhou University) for helpful discussion and for revising the language of the manuscript. We gratefully thank Jingling Shen (Wenzhou University) and Weitao Cong (Wenzhou Medical University) for helpful discussion for revising the manuscript.

Appendix A. Supplementary data

Supplementary data to this article can be found online at https://doi.org/10.1016/j.redox.2022.102481.

References

[1] D.M. Muoio, C.B. Newgard, Mechanisms of disease: molecular and metabolic mechanisms of insulin resistance and β-cell failure in type 2 diabetes, Nat. Rev. Mol. Cell Biol. 9 (2008) 193–205, https://doi.org/10.1038/nrm2327.
[2] N. Apostolova, F. Iannantuoni, A. Gruevska, J. Muntane, M. Rocha, V.M. Victor, Mechanisms of action of metformin in type 2 diabetes: effects on mitochondria and leukocyte-endothelium interactions, Redox Biol. 34 (2020), 101517, https://doi.org/10.1016/j.redox.2020.101517.
[3] M. Foretz, B. Guigas, L. Bertrand, M. Pollak, B. Viollet, Metformin: from mechanisms of action to therapies, Cell Metabol. 20 (6) (2014) 953–966, https://doi.org/10.1016/j.cmet.2014.09.018.
[4] G. Zhou, R. Myers, Y. Li, Y. Chen, X. Shen, J. Fenyk-Melody, M. Wu, J. Ventre, T. Doebber, N. Fujii, N. Musi, M.F. Hirshman, L.J. Goodyear, D.E. Moller, Role of AMP-activated protein kinase in mechanism of metformin action, J. Clin. Invest. 108 (2001) 1167–1174, https://doi.org/10.1172/JCI13505.
[5] L. Agius, B.E. Ford, S.S. Chachra, The metformin mechanism on gluconeogenesis and AMPK activation: the metabolite perspective, Int. J. Mol. Sci. 21 (9) (2020) 3240, https://doi.org/10.3390/ijms21093240.
[6] C.J. Bailey, C. Wilcock, J.H.B. Scarpello, Metformin and the intestine, Diabetologia 51 (8) (2008) 1552–1553, https://doi.org/10.1007/s00125-008-1053-5.
[7] B. Wu, M. Chen, Y. Gao, J. Hu, M. Liu, W. Zhang, W. Huang, In vivo pharmacodynamic and pharmacokinetic effects of metformin mediated by the gut microbiota in rats, Life Sci. 226 (2019) 185–192, https://doi.org/10.1016/j.lfs.2019.04.009.
[8] F. Kristoffer, H. Falk, N. Trine, F. Gwen, L.C. Emmanuelle, S. Shinichi, P. Edi, V. S. Sara, G. Valborg, K.P. Helle, A. Manimozhiyan, K. Karsten, Y.V. Anita, V. Henrik, H. Rajna, I.C. Paul, R.K. Jens, L. Junhua, J. Torben, L. Florence, D. Joël, B. Søren, R. Jeroen, H. Torben, W. Jun, E.S. Dusko, B. Peer, P. Oluf, Disentangling the effects of type 2 diabetes and metformin on the human gut microbiota, Nature 528 (7581) (2015) 262–266, https://doi.org/10.1038/nature15766.
[9] F. Bäckhed, J.K. Manchester, C.F. Semenkovich, J.I. Gordon, Mechanisms underlying the resistance to diet-induced obesity in germ-free mice, P. Natl. Acad. Sci. U. S. A. 104 (3) (2007) 979–984, https://doi.org/10.1073/pnas.0605374104.
[10] H.K. Pedersen, V. Gudmundsdottir, H.B. Nielsen, T. Hyotylainen, T. Nielsen, B. A. Jensen, K. Forslund, F. Hildebrand, E. Prifti, G. Falony, E. Le Chatelier, F. Levenez, J. Doré, I. Mattila, D.R. Plichta, P. Pöhö, L.I. Hellgren, M. Arumugam, S. Sunagawa, S. Vieira-Silva, T. Jørgensen, J.B. Holm, K. Trošt, K. Kristiansen, S. Brix, J. Raes, J. Wang, T. Hansen, P. Bork, S. Brunak, M. Oresic, S.D. Ehrlich, O. Pedersen, Human gut microbes impact host serum metabolome and insulin sensitivity, Nature 535 (7612) (2016) 376–381, https://doi.org/10.1038/nature18646.
[11] W. Jia, G.X. Xie, W.P. Jia, Bile acid-microbiota crosstalk in gastrointestinal inflammation and carcinogenesis, Nat. Rev. Gastroenterol. Hepatol. 15 (2) (2018) 111–128, https://doi.org/10.1038/nrgastro.2017.119.
[12] V. Legry, S. Francque, J.T. Haas, A. Verrijken, C. Sandrine, O. Chávez-Talavera, E. Vallez, L. Vonghia, E. Dirinck, A. Verhaegen, M. Kouach, S. Lestavel, P. Lefebvre, L.V. Gaal, A. Tailleux, R. Paumelle, B. Staels, Bile acid alterations are associated with insulin resistance, but not with NASH, in obese subjects, J. Clin. Endocrinol. Metab. 102 (10) (2017) 3783–3794, https://doi.org/10.1210/jc.2017-01397.
[13] L. Yao, S.C. Seaton, S. Ndousse-Fetter, A.A. Adhikari, N. DiBenedetto, A.I. Mina, A. S. Banks, L. Bry, A.S. Devlin, A selective gut bacterial bile salt hydrolase alters host metabolism, Elife 17 (7) (2018), e37182, https://doi.org/10.7554/eLife.37182.
[14] L.L. Sun, C. Xie, G. Wang, Y. Wu, Q. Wu, X.M. Wang, J. Liu, Y.Y. Deng, J.L. Xia, C. Bo, S.Y. Zhang, Y. Chuyu, G. Lian, X.J. Zhang, H. Zhang, W.H. Bisson, J.M. Shi, X.X. Gao, P.P. Ge, C.H. Liu, W.K. Krausz, R.G. Nicholis, J.W. Cai, B.P. Rimal, A. Patterson, X. Wang, F.J. Gonzalez, C.T. Jiang, Gut microbiota and intestinal FXR mediate the clinical benefits of metformin, Nat. Med. 24 (12) (2018) 1919–1929, https://doi.org/10.1038/s41591-018-0222-4.
[15] E. Sanchez-Rangel, Inzucchi S.E. Metformin, Clinical use in type 2 diabetes, Diabetologia 60 (9) (2017) 1586–1593, https://doi.org/10.1007/s00125-017-4336-x.
[16] Y. Fan, O. Pedersen, Gut microbiota in human metabolic health and disease, Nat. Rev. Microbiol. 19 (1) (2021) 55–71, https://doi.org/10.1038/s41579-020-0433-9.
[17] E.R. McGlone, S.R. Bloom, Bile acids and the metabolic syndrome, Ann. Clin. Biochem. 56 (3) (2019) 326–337, https://doi.org/10.1177/0004563218817798.
[18] N.G. Vallianou, T. Stratigou, S. Tsagarakis, Metformin and gut microbiota: their interactions and their impact on diabetes, Hormones (Basel) 18 (2) (2019) 141–144, https://doi.org/10.1007/s42000-019-00093-w.
[19] D.J. Sansome, C. Xie, S. Veedfald, M. Horowitz, C.K. Rayner, T. Wu, Mechanism of glucose-lowering by metformin in type 2 diabetes: role of bile acids, Diabetes Obes. Metabol. 22 (2) (2020) 141–148, https://doi.org/10.1111/dom.13869.
[20] M. Kars, L. Yang, M.F. Gregor, B.S. Mohammed, T.A. Pietka, B.N. Finck, B. W. Patterson, J.D. Horton, B. Mittendorfer, G.S. Hotamisligil, S. Klein, Tauroursodeoxycholic acid may improve liver and muscle but not adipose tissue insulin sensitivity in obese men and women, Diabetes 59 (8) (2010) 1899–1905, https://doi.org/10.2337/db10-0308.
[21] W.J. Wang, J.F. Zhao, W.F. Gui, D. Sun, H.J. Dai, L. Xiao, H.K. Chu, D. Fan, Q. J. Zhu, S. Bernd, K. Huang, L. Yang, X.H. Hou, Tauroursodeoxycholic acid inhibits intestinal inflammation and barrier disruption in mice with non-alcoholic fatty liver disease, Br. J. Pharmacol. 175 (2018) 469–484, https://doi.org/10.1111/bph.14095.
[22] Y.M. Tao, Y.M. Geng, W.P. Dang, X.X. Xu, H. Zhao, L.J. Zou, Y.S. Li, Mechanism of endoplasmic reticulum stress pathway in the osteogenic phenotypic transformation

of aortic valve interstitial cells, Front. Endocrinol. 13 (2022), 856331, https://doi.org/10.3389/fendo.2022.856331.
[23] R.E. Castro, S. Solá, R. Ramalho, C.J. Steer, C.M.P. Rodrigues, The bile acid tauroursodeoxycholic acid modulates phosphorylation and translocation of bad via phosphatidylinositol 3-kinase in glutamate-induced apoptosis of rat cortical neurons, J. Pharmacol. Exp. Therapeut. 311 (2) (2004) 845–852, https://doi.org/10.1124/jpet.104.070532.
[24] S. Solá, R.E. Castro, P.A. Laires, C.J. Steer, C.M.P. Rodrigues, Tauroursodeoxycholic acid prevents amyloid-beta peptide-induced neuronal death via a phosphatidylinositol 3-kinase-dependent signaling pathway, Mol. Med. 9 (9–12) (2003) 226–234, https://doi.org/10.2119/2003-00042.
[25] Q. Zhu, J.J. Zhong, J.F. Jin, X.M. Yin, Miao H. Tauroursodeoxycholate, A chemical chaperone, prevents palmitate-induced apoptosis in pancreatic β-cells by reducing ER stress, Exp. Clin. Endocrinol. Diabetes 121 (1) (2013) 43–47, https://doi.org/10.1055/s-0032-1321787.
[26] J.A. da Silva, L.S. Figueiredo, J.O. Chaves, K.M. Oliveira, E.M. Carneiro, P. A. Abreu, R.A. Ribeiro, Effects of tauroursodeoxycholic acid on glucose homeostasis: potential binding of this bile acid with the insulin receptor, Life Sci. 285 (2021), 120020, https://doi.org/10.1016/j.lfs.2021.120020.
[27] B. Zou, W. Yang, Y. Tang, Y. Hou, T. Tang, S. Qu, Intestinal microbiota-farnesoid X receptor axis in metabolic diseases, Clin. Chim. Acta 509 (2020) 167–171, https://doi.org/10.1016/j.cca.2020.06.006.
[28] W. Zhang, L. Chen, H. Feng, W. Wang, Y. Cai, F. Qi, X. Tao, J. Liu, Y. Shen, X. Ren, X. Chen, J. Xu, Y. Shen, Rifampicin-induced injury in HepG2 cells is alleviated by TUDCA *via* increasing bile acid transporters expression and enhancing the Nrf2-mediated adaptive response, Free Radic. Biol. Med. 112 (2017) 24–35, https://doi.org/10.1016/j.freeradbiomed.2017.07.003.
[29] S. Moreira, I. Fonseca, M.J. Nunes, A. Rosa, L. Lemos, E. Rodrigues, A.N. Carvalho, T.F. Outeiro, C.M.P. Rodrigues, M.J. Gama, M. Castro-Caldas, Nrf2 activation by tauroursodeoxycholic acid in experimental models of Parkinson's disease, Exp. Neurol. 295 (2017) 77–87, https://doi.org/10.1016/j.expneurol.2017.05.009.
[30] S. Tangvarasittichai, Oxidative stress, insulin resistance, dyslipidemia and type 2 diabetes mellitus, World J. Diabetes 6 (3) (2015) 456–480, https://doi.org/10.4239/wjd.v6.i3.456.
[31] H. Yaribeygi, F.R. Farrokhi, A.E. Butler, A. Sahebkar, Insulin resistance: review of the underlying molecular mechanisms, J. Cell. Physiol. 234 (6) (2019) 8152–8161, https://doi.org/10.1002/jcp.27603.
[32] A. Uruno, Y. Furusawa, Y. Yagishita, T. Fukutomi, H. Muramatsu, T. Negishi, A. Sugawara, T.W. Kensler, M. Yamamoto, The Keap1-Nrf2 system prevents onset of diabetes mellitus, Mol. Cell Biol. 33 (15) (2013) 2996–3010, https://doi.org/10.1128/MCB.00225-13.
[33] H.W.N. Wan, M.K. Kwak, S. Makpol, N.W.S. Wan, Y.A. Mohd Yusof, Piper betle induces phase I & II genes through Nrf2/ARE signaling pathway in mouse embryonic fibroblasts derived from wild type and Nrf2 knockout cells, BMC Compl. Alternative Med. 14 (2014) 72, https://doi.org/10.1186/1472-6882-14-72.
[34] Y.V. Ganesh, G. Negi, S.S. Sharma, A. Kumar, Potential therapeutic effects of the simultaneous targeting of the Nrf2 and NF-κB pathways in diabetic neuropathy, Redox Biol. 1 (1) (2013) 394–397, https://doi.org/10.1016/j.redox.2013.07.005.
[35] D.F. Peng, H. Lu, S.M. Zhu, Z.J. Zhou, T.L. Hu, Z. Chen, A. Zaika, W. El-Rifai, NRF2 antioxidant response protects against acidic bile salts-induced oxidative stress and DNA damage in esophageal cells, Cancer Lett. 458 (2019) 46–55, https://doi.org/10.1016/j.canlet.2019.05.031.
[36] E. Urpilainen, J. Kangaskokko, U. Puistola, P. Karihtala, Metformin diminishes the unfavourable impact of Nrf2 in breast cancer patients with type 2 diabetes, Tumour Biol. 41 (1) (2019), 1010428318815413, https://doi.org/10.1177/1010428318815413.
[37] C.C. Sun, Y.N. Lai, W.H. Wang, X.M. Xu, X.Q. Li, H. Wang, J.Y. Zheng, J.Q. Zheng, Metformin ameliorates gestational diabetes mellitus-induced endothelial dysfunction *via* downregulation of p65 and upregulation of Nrf2, Front. Pharmacol. 11 (2020), e575390, https://doi.org/10.3389/fphar.2020.575390.
[38] J.K. Nicholson, E. Holmes, J. Kinross, R. Burcelin, G. Gibson, W. Jia, S. Pettersson, Host-gut microbiota metabolic interactions, Science 336 (6086) (2012) 1262–1267, https://doi.org/10.1126/science.1223813.
[39] A. Mukherjee, C. Lordan, R.P. Ross, P.D. Cotter, Gut microbes from the phylogenetically diverse genus Eubacterium and their various contributions to gut health, Gut Microb. 12 (1) (2020), 1802866, https://doi.org/10.1080/19490976.
[40] M. Kitahara, F. Takamine, T. Imamura, Y. Benno, Assignment of *Eubacterium sp. VPI 12708* and related strains with high bile acid 7alpha-dehydroxylating activity to *Clostridium scindens* and proposal of *Clostridium hylemonae sp. nov.,* isolated from human faeces, Int. J. Syst. Evol. Microbiol. 50 (3) (2000) 971–978, https://doi.org/10.1099/00207713-50-3-971.
[41] A. Bravard, C. Gérard, C. Defois, B. Benoit, K. Makki, E. Meugnier, D. Rainteau, J. Rieusset, M. Godet, H. Vidal, Metformin treatment for 8 days impacts multiple intestinal parameters in high-fat high-sucrose fed mice, Sci. Rep. 11 (1) (2021), 16684, https://doi.org/10.1038/s41598-021-95117-0.
[42] P. Therdtatha, Y. Song, M. Tanaka, M. Mariyatun, M. Almunifah, N.E.P. Manurung, S. Indriarsih, Y. Lu, K. Nagata, K. Fukami, T. Ikeda, Y.K. Lee, E.S. Rahayu, J. Nakayama, Gut microbiome of Indonesian adults associated with obesity and type 2 diabetes: a cross-sectional study in an Asian city, Yogyakarta, Microorganisms 9 (5) (2021) 897, https://doi.org/10.3390/microorganisms9050897.
[43] I.G. Macchione, L.R. Lopetuso, G. Ianiro, M. Napoli, G. Gibiino, G. Rizzatti, V. Petito, A. Gasbarrini, F. Scaldaferri, *Akkermansia muciniphila*: key player in metabolic and gastrointestinal disorders, Eur. Rev. Med. Pharmacol. Sci. 23 (18) (2019) 8075–8083, https://doi.org/10.26355/eurrev_201909_19024.
[44] H. Plovier, A. Everard, C. Druart, C. Depommier, M. Van Hul, L. Geurts, J. Chilloux, N. Ottman, T. Duparc, L. Lichtenstein, A. Myridakis, N.M. Delzenne, J. Klievink, A. Bhattacharjee, K.C. van der Ark, S. Aalvink, L.O. Martinez, M.E. Dumas, D. Maiter, A. Loumaye, M.P. Hermans, J.P. Thissen, C. Belzer, W.M. de Vos, P. D. Cani, A purified membrane protein from *Akkermansia muciniphila* or the pasteurized bacterium improves metabolism in obese and diabetic mice, Nat. Med. 23 (1) (2017) 107–113, https://doi.org/10.1038/nm.4236.
[45] M.C. Dao, A. Everard, J. Aron-Wisnewsky, N. Sokolovska, E. Prifti, E.O. Verger, B. D. Kayser, F. Levenez, J. Chilloux, L. Hoyles, , Micro ICRO-Obes Consortium, M. E. Dumas, S.W. Rizkalla, J. Doré, P.D. Cani, K. Clément, *Akkermansia muciniphila* and improved metabolic health during a dietary intervention in obesity: relationship with gut microbiome richness and ecology, Gut 65 (3) (2016) 426–436, https://doi.org/10.1136/gutjnl-2014-308778.
[46] H. Ke, F. Li, W. Deng, Z. Li, S. Wang, P. Lv, Y. Chen, Metformin exerts anti-inflammatory and mucus barrier protective effects by enriching *Akkermansia muciniphila* in mice with ulcerative colitis, Front. Pharmacol. 12 (2021), 726707, https://doi.org/10.3389/fphar.2021.726707.
[47] N.R. Shin, J.C. Lee, H.Y. Lee, M.S. Kim, T.W. Whon, M.S. Lee, J.W. Bae, An increase in the *Akkermansia spp.* population induced by metformin treatment improves glucose homeostasis in diet-induced obese mice, Gut 63 (5) (2014) 727–735, https://doi.org/10.1136/gutjnl-2012-303839.